Supplementary Material

Figure S1

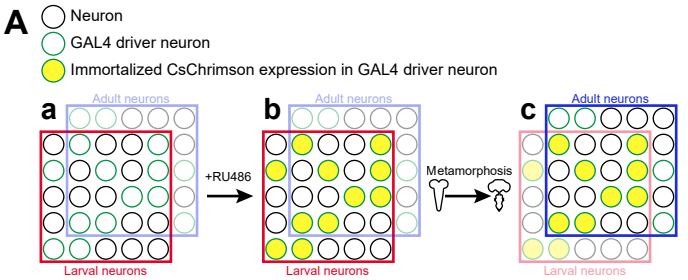
A
Neuron
GAL4 driver neuron
Immortalized CsChrimson expression in GAL4 driver neuron
a
Adult neurons
Larval neurons
+RU486
b
Adult neurons
Larval neurons
Metamorphosis
c
Adult neurons
Larval neurons

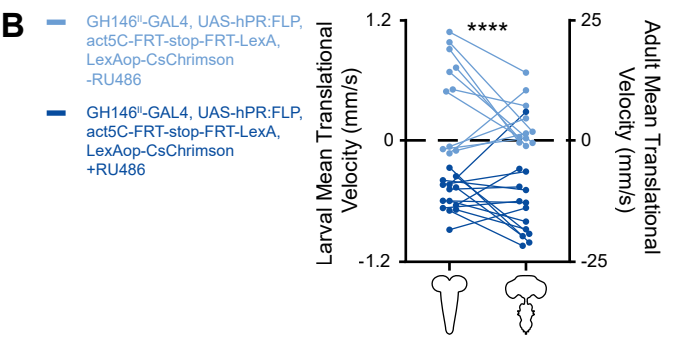
B
GH146II-GAL4, UAS-hPR:FLP, act5C-FRT-stop-FRT-LexA, LexAop-CsChrimson -RU486
GH146II-GAL4, UAS-hPR:FLP, act5C-FRT-stop-FRT-LexA, LexAop-CsChrimson +RU486
Larval Mean Translational Velocity (mm/s)
Adult Mean Translational Velocity (mm/s)
1.2
0
-1.2
25
0
-25
****

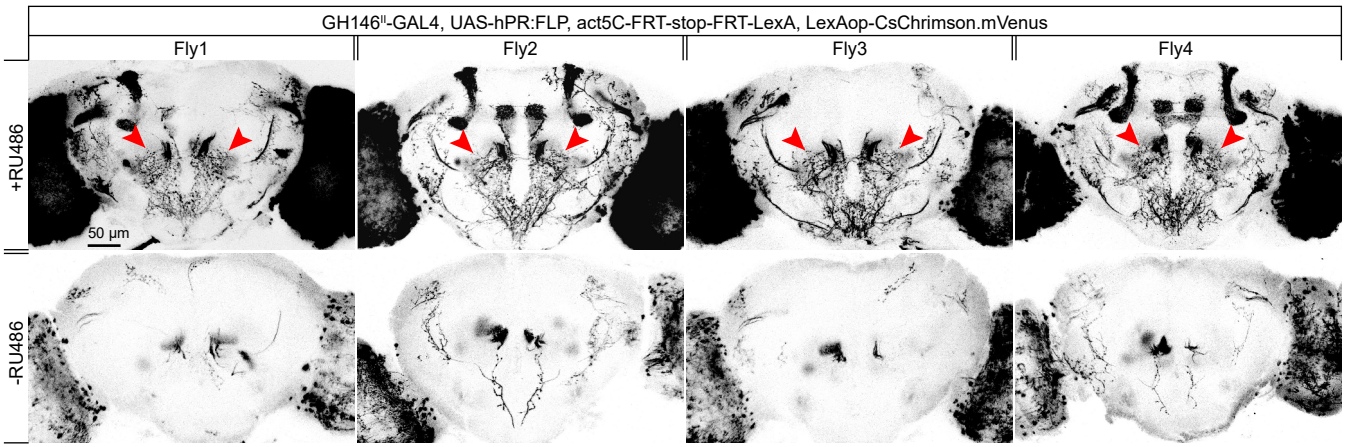
C
GH146II-GAL4, UAS-hPR:FLP, act5C-FRT-stop-FRT-LexA, LexAop-CsChrimson.mVenus
Fly1
Fly2
Fly3
Fly4
+RU486
-RU486
50 µm

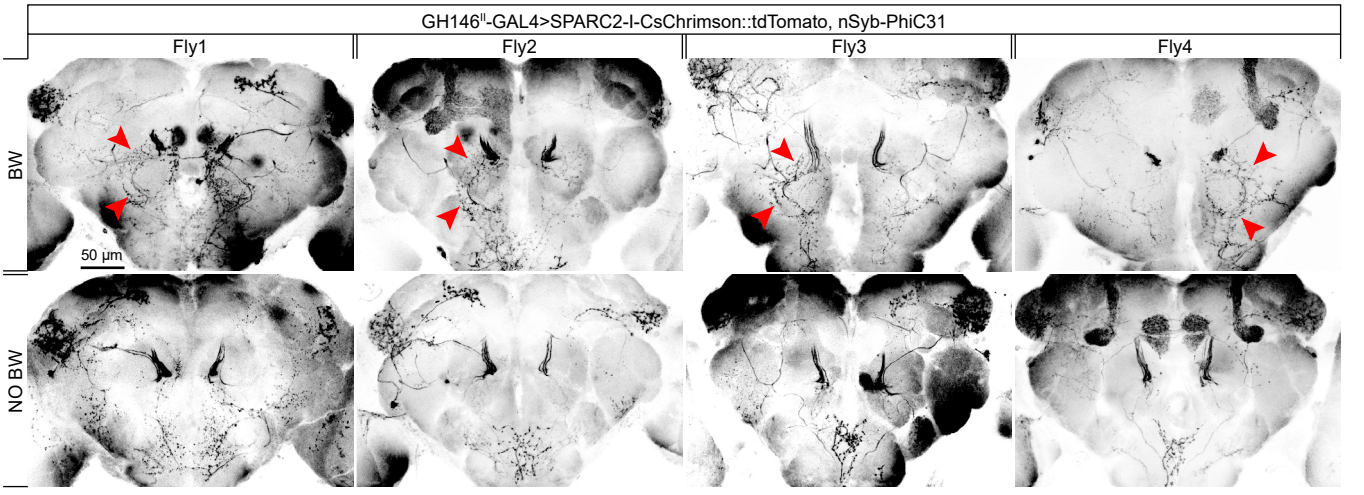
D
GH146II-GAL4>SPARC2-I-CsChrimson::tdTomato, nSyb-PhiC31
Fly1
Fly2
Fly3
Fly4
BW
NO BW
50 µm

Figure S1: MooSEZ survives metamorphosis and maintains its functional role along development.

(**A**) Schematic description of the immortalization genetic technique utilized to reveal whether larval MooSEZ persists through metamorphosis. (a) During larval stages, a GAL4 driver line labels subset of neurons (green circles) within the entire larval cell population (black and green circles confined by a red square). Adult-specific neurons are not labeled (faded black and green circles confined by a faded blue square). (b) Upon application of RU-486 during larval stages, RU-486 inducible flippase (hPR:FLP), expressed in neurons labeled by the GAL4 driver line, removes an intervening stop sequence from Actin-FRT-STOP-FRT-LexA. Following this reaction, constitutive LexA activity leads to permanent LexAop-CsChrimson-mVenus expression in neurons targeted by the GAL4 driver (yellow-filled green circles). (c) During the transition from larva to adult, some of the embryonic-born larval neurons die (faded yellow-filled green and faded black circles confined by a faded red square), while other immature larval neurons acquire their identity and function as adult-specific (green and black circles confined by a blue square). In addition, other neuronal subsets persist through metamorphosis and function at both larval and adult stages (black and green circles confined by both blue and faded red squares). At the adult stage, the GAL4 driver line targets subsets of adult-specific (green circles) as well as developmentally-conserved neurons already marked by CsChrimson-mVenus expression during early larval stages (yellow-filled green circles).

(**B**) Mean translational velocity following optogenetic activation (larvae, 9-s; adults, 2-s) of single larvae and their matched adult flies in which GH146^{II}-GAL4 neurons were either immortalized by hPR:FLP (dark blue) or not (light blue) during larval stages. Immortalization was obtained by the expression of LexAop-CsChrismon following the removal of the stop cassette from act5C-FRT-STOP-FRT-LexA. Individual larvae subjected to RU-486 exhibited optogenetically-induced backward locomotion that was also observed for their respective adult flies, whereas RU-486 untreated single larvae showed lack of backward locomotion at both larval and subsequent adult stages ($11 \leq n \leq 14$, **** $p < 0.0001$ for main effect for RU-486 treatment, repeated measures two-way ANOVA). Larva and adult results used for this panel are identical to the results used for Figure 1F.

(**C**) Top, expression patterns of representative adult fly brains expressing immortalized LexAop-CsChrimson-mVenus in GH146^{II}-GAL4 neurons following application of RU-486 during larval stages. Red arrowheads signify MooSEZ arborizations in the SPZ. MooSEZ labeling is consistently observed in brains of adult flies exposed to RU-486 during larval stages. Bottom, expression patterns of representative brains of adult flies that were not exposed to RU-486 during larval stages. While some leaked LexAop-CsChrismon-mVenus expression is observed in subset of GH146-GAL4^{II} neurons, MooSEZ labeling is not detected. Maximum intensity projections of 20 (top) and 30 (bottom) confocal sections (1 µm), obtained from similar coronal planes within the central brain, are presented. Scale bar applies to all images.

(**D**) Top, expression patterns of representative SPARC mosaic brains of adult flies expressing CsChrimson::tdTomato in a stochastically distributed subsets of neurons within GH146^{II}-GAL4 driver line which performed backward locomotion following optogenetic stimulation at both larval and adult stages. MooSEZ arborizations are designated by red arrowheads. MooSEZ labeling is consistently detected in these fly brains. Bottom, expression patterns of representative SPARC mosaic brains of adult flies expressing CsChrimson::tdTomato in a stochastically distributed subsets of neurons within GH146^{II}-GAL4 driver line which showed lack of backward locomotion upon optogenetic activation at both larval and adult stages. Consistent lack of tdTomato expression in MooSEZ is observed in these fly brains. Maximum intensity projections of 30-55 (top) and 50 (bottom) confocal sections (1 µm), obtained from similar coronal planes within the central brain, are presented. Scale bar applies to all images.

For details of statistical analysis, see Table S1.

Figure S2

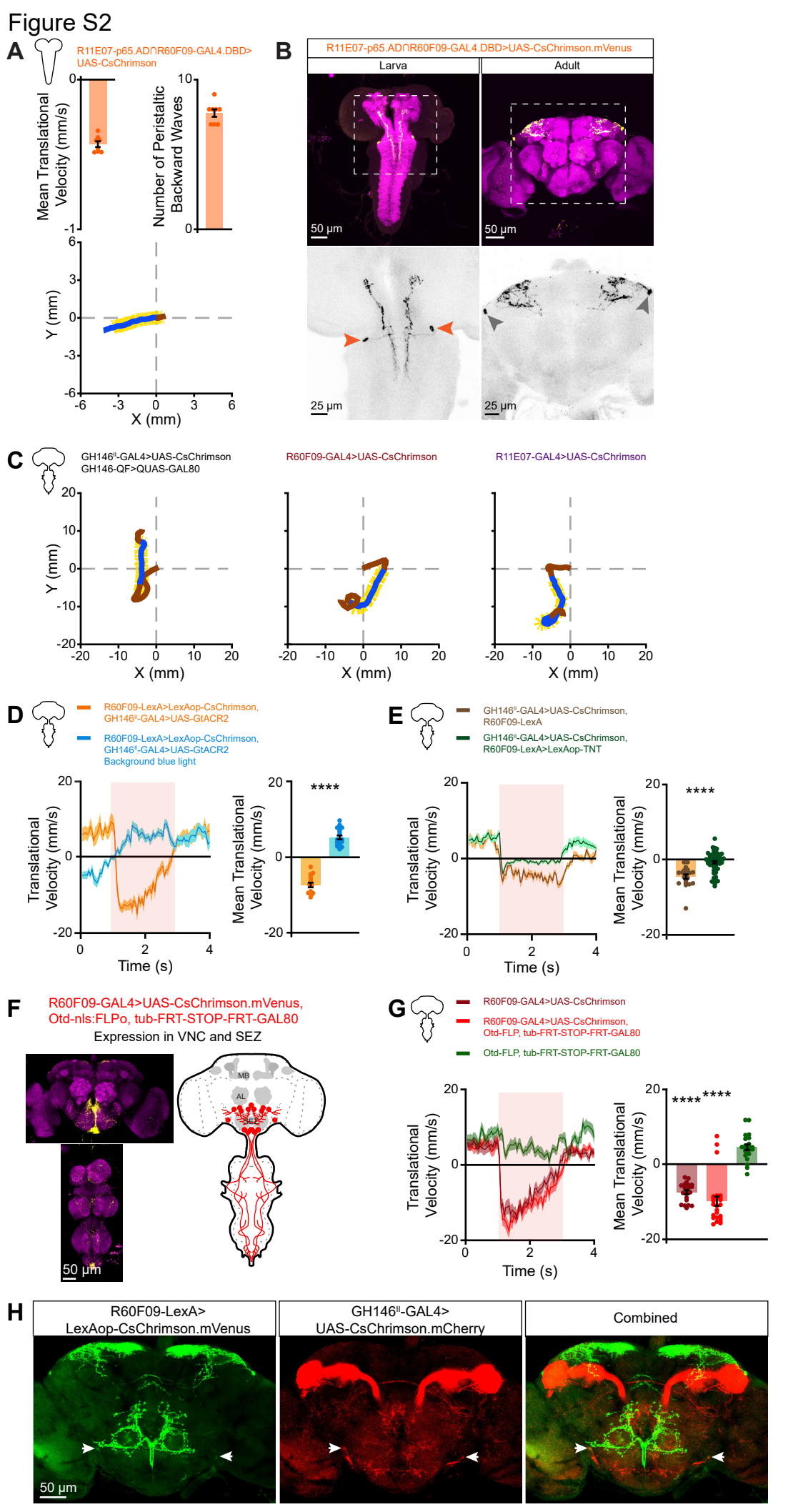
A
R11E07-p65.AD∩R60F09-GAL4.DBD>
UAS-CsChrimson
Mean Translational Velocity (mm/s)
Number of Peristaltic Backward Waves
Y (mm)
X (mm)
B
R11E07-p65.AD∩R60F09-GAL4.DBD>UAS-CsChrimson.mVenus
Larva
Adult
50 µm
25 µm
C
GH146II-GAL4>UAS-CsChrimson
GH146-QF>QUAS-GAL80
R60F09-GAL4>UAS-CsChrimson
R11E07-GAL4>UAS-CsChrimson
Y (mm)
X (mm)
D
R60F09-LexA>LexAop-CsChrimson,
GH146II-GAL4>UAS-GtACR2
R60F09-LexA>LexAop-CsChrimson,
GH146II-GAL4>UAS-GtACR2
Background blue light
Translational Velocity (mm/s)
Mean Translational Velocity (mm/s)
****
Time (s)
E
GH146II-GAL4>UAS-CsChrimson,
R60F09-LexA
GH146II-GAL4>UAS-CsChrimson,
R60F09-LexA>LexAop-TNT
Translational Velocity (mm/s)
Mean Translational Velocity (mm/s)
****
Time (s)
F
R60F09-GAL4>UAS-CsChrimson.mVenus,
Otd-nls:FLPo, tub-FRT-STOP-FRT-GAL80
Expression in VNC and SEZ
MB
AL
SEZ
50 µm
G
R60F09-GAL4>UAS-CsChrimson
R60F09-GAL4>UAS-CsChrimson,
Otd-FLP, tub-FRT-STOP-FRT-GAL80
Otd-FLP, tub-FRT-STOP-FRT-GAL80
Translational Velocity (mm/s)
Mean Translational Velocity (mm/s)
****
****
Time (s)
H
R60F09-LexA>
LexAop-CsChrimson.mVenus
GH146II-GAL4>
UAS-CsChrimson.mCherry
Combined
50 µm

Figure S2: R60F09-GAL4 driver line elicits adult backward locomotion via MooSEZ.
(**A**) Top, mean translational velocity (left) and number of peristaltic backward waves (right) of larval crawling during a 9-s red light pulse for AMB-split GAL4 driving UAS-CsChrimson. Bottom, example of single larva crawling trajectory for AMB-split GAL4 driving UAS-CsChrimson before, during and after optogenetic stimulation. 9-s red light pulse is designated by yellow, blue denotes backward crawling, and brown forward motion. The (0, 0) coordinate represents larvae's trajectory onset at t=0. Larval AMB split GAL4 backward retreat highly resembles the behavioral responses observed for GH146^{II}-, NP225-, NP5288, and GH146^{II}-GAL4 with subtracted GH146-QF larvae (Figures 1A, 1B, and 1D) following optogenetic stimulation (n=8).
(**B**) Top, expression pattern of AMB split GAL4 driving UAS-CsChrimson.mVenus in larva (top left) and adult (top right). Bottom, Enlargement of the brain regions demarcated by the dashed outlines above. Maximum intensity projections of 95 (top left), 120 (top right), 44 (bottom left), and 90 (bottom right) confocal sections (1 µm) are presented. Larval AMB (bottom left) and adult bilateral LH neuron (bottom right) are designated by orange and gray arrowheads respectively.
During larval stages, AMB split GAL4 labels the AMBs whose cell bodies lie within the same region as the larval SEZ somata marked by GH146^{II}-GAL4 with subtracted GH146-QF (Figure 1E). By contrast, during adulthood AMB spilt GAL4 driver does not target the SEZ, but rather a paired LH neuron.
(**C**) Examples of single fly walking trajectories for GH146^{II}-GAL4 intersected with GH146-QF, R60F09-GAL4, and R11E07-GAL4 driving CsChrimson before, during and after optogenetic stimulation. 2-s red light pulse is designated by yellow, blue denotes backward walking and brown forward motion. The (0, 0) coordinate represents flies' trajectory onset at t=0. A short 2-s optogenetic activation of flies expressing CsChrimson using GH146^{II}-GAL4 with subtracted GH146-QF, R60F09-GAL4, and R11E07-GAL4 driver lines elicits a similar motor response of persistent backward retreat across the three driver lines.
(**D**) Left, translational velocity ± SEM (shading) of adult flies following optogenetic activation of R60F09 neurons with CsChrimson (yellow) or when the inhibitory GtACR2 channel was co-activated in GH146^{II}-GAL4 neurons (blue). The red light activating CsChrimson was provided between the first and the third seconds, while the blue light activating GtACR2 was provided during the first three seconds. The 2-s red light pulse is labeled in light red. GH146^{II}-GAL4 was used to drive UAS-GtACR2 and R60F09-LexA was used to drive LexAop-CsChrimson. Silencing GH146^{II}-GAL4 neurons using GtACR2 abolishes R60F09-triggered backward locomotion. Right, mean translational velocity during the 2-s red light pulse obtained from traces on the left. A significant difference is observed between the mean translational velocities generated upon optogenetic activation of R60F09 neurons with the co-activation of GtACR2 and without the co-activation of GtACR2 in GH146^{II} neurons ($16 \leq n \leq 20$, **** $p < 0.0001$, Mann-Whitney test).
(**E**) Left, translational velocity ± SEM (shading) of adult flies following optogenetic activation of GH146^{II} neurons with CsChrimson in the presence (green) or absence (brown) of TNT in R60F09 neurons. The 2-s red light pulse activating CsChrimson is labeled in light red. GH146^{II}-GAL4 was used to drive UAS-CsChrimson and R60F09-LexA was used to drive LexAop-TNT (when required). Silencing R60F09-LexA neurons using TNT significantly suppresses GH146^{II}-GAL4-triggered backward walking. Right, mean translational velocity during the 2-s red light pulse obtained from traces on the left. A significant difference is observed between the mean translational velocities during optogenetic activation of GH146^{II} neurons when TNT is expressed and when TNT is not expressed in the neurons labeled by R60F09 ($20 \leq n \leq 59$, **** $p < 0.0001$, Mann-Whitney test).
(**F**) Left, expression pattern of R60F09-GAL4 driving UAS-CsChrimson.mVenus in the presence of Otd-nls:FLPo, and tub-FRT-STOP-FRT-GAL80 in adult flies. CsChrimson.mVenus was used to label the cells. Maximum intensity projection of 135 confocal sections (1 µm) through the central brain and VNC are presented. Scale bar applies to both images. CsChrimson expression in the VNC originates primarily from labeled SEZ descending neurons. Right, schematic drawing of the

expression pattern of CsChrimson obtained by intersecting R60F09-GAL4 with Otd-nls:FLPo, and tub-FRT-STOP-FRT-GAL80.
(**G**) Left, translational velocity ± SEM (shading) of adult flies following optogenetic activation of R60F09-GAL4 driving UAS-CsChrimson (dark red), R60F09-GAL4 driving UAS-CsChrimson in the presence of both Otd-nls:FLPo and tub-FRT-STOP-FRT-GAL80 (red), and Otd-nls:FLPo, tub-FRT-STOP-FRT-GAL80 control (green). The 2-s light pulse is labeled in light red. Right, mean translational velocity during the 2-s light pulse obtained from traces on the left. Optogenetic activation of R60F09-GAL4 SEZ neurons does not lead to reduction in backward locomotion ($21 \leq n \leq 25$, **** $p < 0.0001$ for pairwise comparisons of Otd-nls:FLPo, tub-FRT-STOP-FRT-GAL80 control with each experimental group, Kruskal - Wallis test followed by Dunn's post-hoc tests).
(**H**) Expression pattern of R60F09-LexA (left), GH146^{II}-GAL4 (middle), and both driver lines (right) in the adult fly brain. R60F09-LexA was used to drive LexAop-CsChrimson.mVenus and GH146^{II}-GAL4 was used to drive UAS-CsChrimson.mCherry. A clear overlap between the two driver lines is observed in a paired lateral SEZ neuron (right). White arrowheads mark the cell bodies of the paired lateral SEZ neuron targeted by both driver lines. Maximum intensity projections of 20 confocal sections (1 µm) through the central brain are presented. Scale bar applies to all images. For details of statistical analysis, see Table S1.

Figure S3

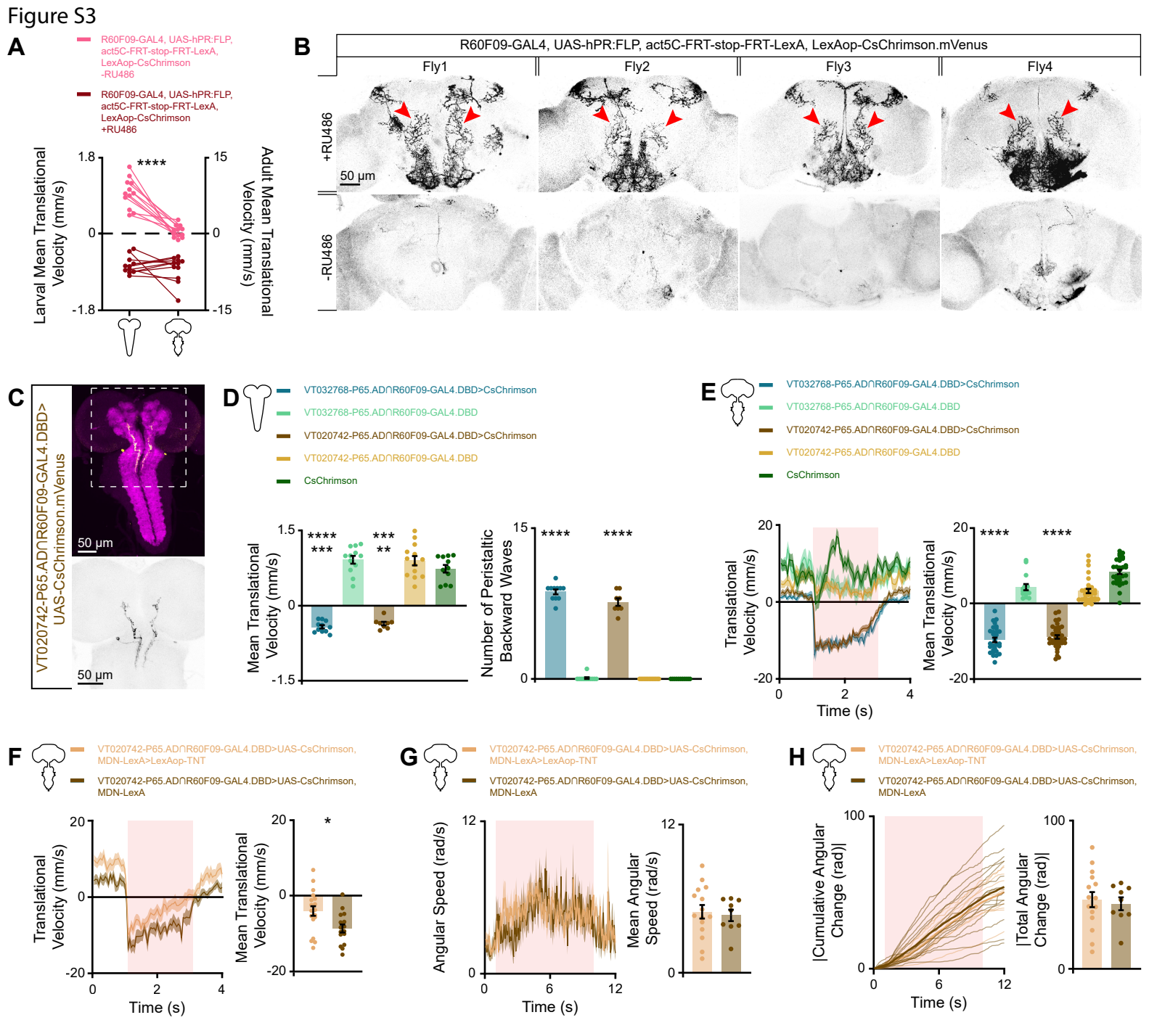
A
R60F09-GAL4, UAS-hPR:FLP, act5C-FRT-stop-FRT-LexA, LexAop-CsChrimson -RU486
R60F09-GAL4, UAS-hPR:FLP, act5C-FRT-stop-FRT-LexA, LexAop-CsChrimson +RU486
Larval Mean Translational Velocity (mm/s)
Adult Mean Translational Velocity (mm/s)
****
B
R60F09-GAL4, UAS-hPR:FLP, act5C-FRT-stop-FRT-LexA, LexAop-CsChrimson.mVenus
Fly1
Fly2
Fly3
Fly4
+RU486
-RU486
50 µm
C
VT020742-P65.ADnR60F09-GAL4.DBD> UAS-CsChrimson.mVenus
50 µm
D
VT032768-P65.ADnR60F09-GAL4.DBD>CsChrimson
VT032768-P65.ADnR60F09-GAL4.DBD
VT020742-P65.ADnR60F09-GAL4.DBD>CsChrimson
VT020742-P65.ADnR60F09-GAL4.DBD
CsChrimson
Mean Translational Velocity (mm/s)
Number of Peristaltic Backward Waves
E
VT032768-P65.ADnR60F09-GAL4.DBD>CsChrimson
VT032768-P65.ADnR60F09-GAL4.DBD
VT020742-P65.ADnR60F09-GAL4.DBD>CsChrimson
VT020742-P65.ADnR60F09-GAL4.DBD
CsChrimson
Translational Velocity (mm/s)
Time (s)
Mean Translational Velocity (mm/s)
F
VT020742-P65.ADnR60F09-GAL4.DBD>UAS-CsChrimson, MDN-LexA>LexAop-TNT
VT020742-P65.ADnR60F09-GAL4.DBD>UAS-CsChrimson, MDN-LexA
Translational Velocity (mm/s)
Time (s)
Mean Translational Velocity (mm/s)
G
VT020742-P65.ADnR60F09-GAL4.DBD>UAS-CsChrimson, MDN-LexA>LexAop-TNT
VT020742-P65.ADnR60F09-GAL4.DBD>UAS-CsChrimson, MDN-LexA
Angular Speed (rad/s)
Time (s)
Mean Angular Speed (rad/s)
H
VT020742-P65.ADnR60F09-GAL4.DBD>UAS-CsChrimson, MDN-LexA>LexAop-TNT
VT020742-P65.ADnR60F09-GAL4.DBD>UAS-CsChrimson, MDN-LexA
|Cumulative Angular Change (rad)|
Time (s)
|Total Angular Change (rad)|

Figure S3: Selective MooSEZ activation using MooSEZ-specific split-GAL4 drivers.
(**A**) Mean translational velocity following optogenetic activation (larvae, 9-s; adults, 2-s) of single larvae and their matched adult flies in which R60F09-GAL4 neurons were either immortalized by hPR:FLP (dark red) or not (light red) during larval stages. Immortalization was obtained by the expression of LexAop-CsChrismon following the removal of the stop cassette from act5C-FRT-STOP-FRT-LexA. Individual larvae subjected to RU-486 exhibited optogenetically-induced backward locomotion that was also observed for their respective adult flies, whereas RU-486 untreated single larvae showed lack of backward locomotion at both larval and subsequent adult stages ($11 \leq n \leq 12$, **** $p < 0.0001$ for main effect for RU-486 treatment, repeated measures two-way ANOVA). Larva and adult results used for this panel are identical to the results used for Figure 3D.
(**B**) Top, expression patterns of representative adult fly brains expressing immortalized LexAop-CsChrimson-mVenus in R60F09-GAL4 neurons following application of RU-486 during larval stages. Red arrowheads signify MooSEZ arborizations in the SPZ. MooSEZ labeling is consistently observed in brains of adult flies exposed to RU-486 during larval stages. Bottom, expression patterns of representative brains of adult flies that were not exposed to RU-486 during larval stages. Consistent lack of mVenus expression in the vast majority of R60F09-GAL4 neurons, and in particular in MooSEZ, is observed. Maximum intensity projections of 50-80 (top) and 80 (bottom) confocal sections (1 µm), obtained from similar coronal planes within the central brain, are presented. Scale bar applies to all images.
For details of statistical analysis, see Table S1.
(**C**) Top, expression pattern of MooSEZ expressing CsChrimson.mVenus in larval nervous system. MooSEZ-specific split GAL4 driver line (VT020742-p65.AD∩R60F09-GAL4.DBD) was used to drive UAS-CsChrimson.mVenus. Maximum intensity projection of 90 confocal section (1 µm) is presented. Bottom, Enlargement of the region demarcated by the dashed outline above. Maximum intensity projection of 50 confocal sections (1 µm) is presented. Combining GAL4 hemidrivers VT020742 and R60F09 leads to GAL4 expression exclusively in larval MooSEZs.
(**D**) Left, mean translational velocity of larval crawling during a 9-s red light pulse for MooSEZ split GAL4 driver lines, and their respective parental controls as designated. The split GAL4 driver lines VT032768-p65.AD∩R60F09-GAL4.DBD, and VT020742-p65.AD∩R60F09-GAL4.DBD, were used to drive CsChrimson in MooSEZs. Pronounced backward crawling is observed during the 9-s light pulse for MooSEZ split-GAL4 larvae, but not for their respective parental controls ($8 \leq n \leq 13$, ** $p < 0.01$, *** $p < 0.001$, **** $p < 0.0001$ for pairwise comparisons with respective parental controls, Kruskal - Wallis test followed by Dunn's post-hoc tests). Right, Number of peristaltic backward waves during a 9-s red light pulse for MooSEZ split GAL4 driver lines, and their respective parental controls as designated. Number of peristaltic waves of muscle contractions travelling from anterior to posterior abdominal segments of the larva is significantly greater in larvae expressing CsChrimson driven by MooSEZ split GAL4 drivers, than in respective parental control larvae ($8 \leq n \leq 13$, **** $p < 0.0001$ for pairwise comparisons with respective parental controls, Kruskal - Wallis test followed by Dunn's post-hoc tests).
(**E**) Left, translational velocity ± SEM (shading) of adult flies following optogenetic activation of MooSEZ split GAL4 driver lines, and their respective parental controls as designated. The split GAL4 driver lines VT032768-p65.AD∩R60F09-GAL4.DBD, and VT020742-p65.AD∩R60F09-GAL4.DBD, were used to drive UAS-CsChrimson in MooSEZs. The 2-s light pulse is labeled by light red. Optogenetic activation of both MooSEZ split GAL4 driver lines elicits pronounced motor response of backward walking. Right, mean translational velocity during the 2-s light pulse obtained from traces on the left. Activation of CsChrimson using MooSEZ split GAL4 driver lines leads to significant motor response of backward walking, which is not observed for parental control flies ($15 \leq n \leq 38$, **** $p < 0.0001$, Kruskal - Wallis test followed by Dunn's post-hoc tests).

(**F**) Left, translational velocity ± SEM (shading) of adult flies following optogenetic activation of MooSEZs in the presence (light brown) or absence (dark brown) of TNT in MDNs. MooSEZ-specific split GAL4 driver (VT020742-p65.ADꓵR60F09-GAL4.DBD) was used to drive UAS-CsChrimson in MooSEZs, and MDN-LexA driver (VT44845-LexA) was used to drive LexAop-TNT in MDNs (when required). The 2-s light pulse is labeled in light red. Right, mean translational velocity during the 2-s light pulse obtained from traces on the left. As previously reported for GH146^{II}-GAL4 neurons(*37*), backward locomotion is reduced but not abolished in flies expressing TNT in MDNs upon MooSEZ stimulation (16≤n≤19, * $p < 0.05$, Mann-Whitney test).

(**G**) Left, Angular speed ± SEM (shading) of adult flies following a 9-s long optogenetic stimulation of MooSEZs in the presence (light brown) or absence (dark brown) of TNT in MDNs. MooSEZ-specific split GAL4 driver (VT020742-p65.ADꓵR60F09-GAL4.DBD) was used to drive UAS-CsChrimson in MooSEZs, and MDN-LexA driver (VT44845-LexA) was used to drive LexAop-TNT in MDNs (when required). The light pulse is labeled in light red. Right, mean angular speed during the 9-s light pulse obtained from traces on the left. Continuous MooSEZ activation results in persistent MDN-independent rotational responses, as was also observed for activation of GH146^{II}-GAL4 neurons(*37*) (9≤n≤15, Mann-Whitney test).

(**H**) Single fly traces (light) of absolute cumulative angular change and their respective means (dark) following a 9-s long optogenetic activation of MooSEZs in the presence (light brown) or absence (dark brown) of TNT in MDNs. MooSEZ-specific split GAL4 driver (VT020742-p65.ADꓵR60F09-GAL4.DBD) was used to drive UAS-CsChrimson in MooSEZs, and MDN-LexA driver (VT44845-LexA) was used to drive LexAop-TNT in MDNs (when required). The light pulse is labeled in light red. Right, absolute total angular change at the end of the 9-s red light pulse obtained from traces on the left. The angular component elicited by activation of MooSEZs is not mediated by MDNs, as was also observed for excitation of GH146^{II}-GAL4 neurons(*37*) (9≤n≤15, Mann-Whitney test).

For details of statistical analysis, see Table S1.

Figure S4

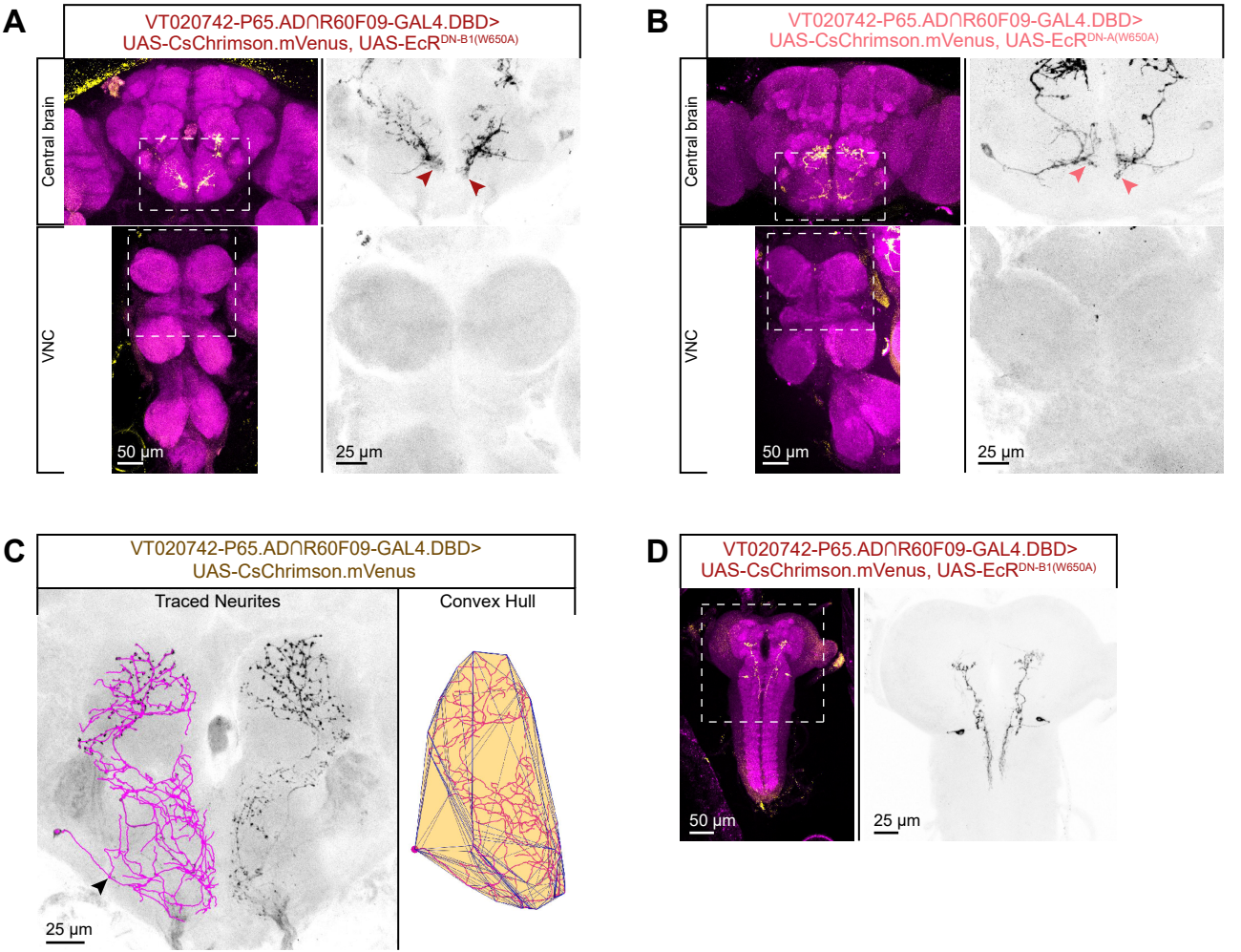
A
VT020742-P65.AD∩R60F09-GAL4.DBD>
UAS-CsChrimson.mVenus, UAS-EcR^DN-B1(W650A)
Central brain
VNC
50 µm
25 µm
B
VT020742-P65.AD∩R60F09-GAL4.DBD>
UAS-CsChrimson.mVenus, UAS-EcR^DN-A(W650A)
Central brain
VNC
50 µm
25 µm
C
VT020742-P65.AD∩R60F09-GAL4.DBD>
UAS-CsChrimson.mVenus
Traced Neurites
Convex Hull
25 µm
D
VT020742-P65.AD∩R60F09-GAL4.DBD>
UAS-CsChrimson.mVenus, UAS-EcR^DN-B1(W650A)
50 µm
25 µm

Figure S4: Perturbing ecdysone signaling within MooSEZ neither eliminates pruning nor affects larval morphology.

(**A**) Left, expression pattern of adult MooSEZ expressing CsChrimson.mVenus and $EcR^{DN\text{-}B1(W650A)}$ in the central brain (top) and VNC (bottom). MooSEZ-specific split GAL4 driver line (VT020742-p65.ADꓵR60F09-GAL4.DBD) was used to drive UAS-CsChrimson.mVenus and UAS-$EcR^{DN\text{-}B1(W650A)}$. Maximum intensity projections of 70 confocal sections (1 µm) through the central brain and VNC are presented. Scale bar applies to both images. Right, Enlargement of the regions demarcated by the dashed outlines on the left for the central brain (top) and VNC (bottom). Maximum intensity projections of 60 confocal sections (1 µm) are presented. Scale bar applies to both images. Arrowheads indicate pruned MooSEZ neurites in the adult SEZ. Both adult central brain and VNC show lack of unpruned neurites.

(**B**) Left, expression pattern of adult MooSEZ expressing CsChrimson.mVenus and $EcR^{DN\text{-}A(W650A)}$ in the central brain (top) and VNC (bottom). MooSEZ-specific split GAL4 driver line (VT020742-p65.ADꓵR60F09-GAL4.DBD) was used to drive UAS-CsChrimson.mVenus and UAS-$EcR^{DN\text{-}A(W650A)}$. Maximum intensity projections of 100 confocal sections (1 µm) through the central brain and VNC are presented. Scale bar applies to both images. Right, Enlargement of the regions demarcated by the dashed outlines on the left for the central brain (top) and VNC (bottom). Maximum intensity projections of 60 confocal sections (1 µm) are presented. Scale bar applies to both images. Arrowheads indicate pruned MooSEZ neurites in the adult SEZ. Both adult central brain and VNC show lack of unpruned neurites.

(**C**) Left, representative example for traced MooSEZ neurites used for visualization and quantification of adult MooSEZ morphology as presented in Figures 5G-5N. For visualization purposes, the traced structure of only one of the paired MooSEZs is displayed. Arrowhead indicates the first branching point along MooSEZ primary branch. Cable length metric (Figure 5L) was computed as the sum of all MooSEZ traced branches. Number of branch points metric (Figure 5M) was computed as the total number of branch points along MooSEZ traced segments. Maximum intensity projection of 105 confocal sections (1 µm) through the central brain is presented. Right, representative example for three-dimensional convex hull of the traced MooSEZ presented on the left used for quantification of adult MooSEZ morphology as presented in Figure 5N. Convex hull size was computed as the volume of the smallest convex polyhedron enclosing MooSEZ traced structure. The yellow fill within the polyhedron shape indicates its volume.

(**D**) Left, expression pattern of larval MooSEZ expressing CsChrimson.mVenus in the presence of $EcR^{DN\text{-}B1(W650A)}$. MooSEZ-specific split GAL4 driver line (VT020742-p65.ADꓵR60F09-GAL4.DBD) was used to drive UAS-CsChrimson.mVenus and UAS-$EcR^{DN\text{-}B1(W650A)}$. Maximum intensity projection of 80 confocal sections (1 µm) is presented. Right, Enlargement of the region demarcated by the dashed outline on the left. Maximum intensity projection of 35 confocal sections (1 µm) is presented. $EcR^{DN\text{-}B1(W650A)}$ expression does not affect MooSEZ morphology during larval development.

Supplemental video legends

Video S1: Broad PN driver lines elicit backward crawling.
Example of backward locomotion following a 9-s red light (617 nm) pulse in larvae expressing CsChrimson under the control of the broad PN driver line NP225-GAL4.

Video S2: MooSEZ rotational component is added to the motor response following metamorphosis.
Left, example of straight backward locomotion of $GH146^{II}$-GAL4 SPARC mosaic larva expressing CsChrimson in the right MooSEZ following a 2-s red light (617 nm) stimulation. Right, example of ipsilateral backward rotation of $GH146^{II}$-GAL4 SPARC mosaic fly developed from the larva presented on the left expressing CsChrimson in the right MooSEZ during a 2-s red light (617 nm) stimulation.

Video S3: AMB split GAL4 parental driver lines elicit backward walking in adult flies.
Left, example of backward walking following a 2-s red light (617nm) pulse in flies expressing CsChrimson under the control of the GAL4 driver R60F09-GAL4. Right, example of backward walking following a 2-s red light (617nm) pulse in flies expressing CsChrimson under the control of the GAL4 driver R11E07-GAL4.

Video S4: MooSEZ split GAL4 driver lines trigger robust backward locomotion in both larva and adult.
Left, example of backward locomotion of a single larva expressing CsChrimson driven by MooSEZ-specific GAL4 driver line (VT020742-p65.ADꓵR60F09-GAL4.DBD) following a 2-s red light (617 nm) stimulation. Right, example of backward locomotion of a single adult fly developed from the larva presented on the left expressing CsChrimson driven by MooSEZ-specific GAL4 driver line (VT020742-p65.ADꓵR60F09-GAL4.DBD) following a 2-s red light (617 nm) stimulation.

Video S5: $ECR^{DN\text{-}B1(W650A)}$ expression in MooSEZ abolishes adult backward walking.
Left, example of backward locomotion of flies expressing CsChrimson using MooSEZ-specific GAL4 driver line (VT020742-p65.ADꓵR60F09-GAL4.DBD) following a 2-s red light (617 nm) stimulation. Right, example of lack of backward locomotion of flies expressing CsChrimson and $ECR^{DN\text{-}B1(W650A)}$ using MooSEZ-specific GAL4 driver line (VT020742-p65.ADꓵR60F09-GAL4.DBD) following a 2-s red light (617 nm) stimulation.

Supplemental table

Table S1: Statistical analysis, related to Figures 1-3, 5, and S1-S3.

Table S1: Statistical Analysis

Figure	Data	Statistical method	Comparison	*p*-value	FDR-adjusted *p*-value	Significance
Figure 1B	Mean Translational Velocity	Kruskal-Wallis test	1. GH146-GAL4>UAS-CsChrimson (n=12) 2. GH146-GAL4 (n=11) 3. NP225-GAL4>UAS-CsChrimson (n=13) 4. NP225-GAL4 (n=10) 5. NP5288-GAL4>UAS-CsChrimson (n=13) 6. NP5288-GAL4 (n=11) 7. UAS-CsChrimson (n=11)	<0.0001	-	****
	Mean Translational Velocity	Dunn's multiple comparisons test	1. GH146-GAL4>UAS-CsChrimson (n=12) 2. GH146-GAL4 (n=11)	<0.0001	<0.0001	****
	Mean Translational Velocity	Dunn's multiple comparisons test	1. GH146-GAL4>UAS-CsChrimson (n=12) 2. UAS-CsChrimson (n=11)	<0.0001	<0.0001	****
	Mean Translational Velocity	Dunn's multiple comparisons test	1. NP225-GAL4>UAS-CsChrimson (n=13) 2. NP225-GAL4 (n=10)	0.00065	0.00065	***
	Mean Translational Velocity	Dunn's multiple comparisons test	1. NP225-GAL4>UAS-CsChrimson (n=13) 2. UAS-CsChrimson (n=11)	<0.0001	<0.0001	****
	Mean Translational Velocity	Dunn's multiple comparisons test	1. NP5288-GAL4>UAS-CsChrimson (n=13) 2. NP5288-GAL4 (n=11)	0.00011	0.00013	***
	Mean Translational Velocity	Dunn's multiple comparisons test	1. NP5288-GAL4>UAS-CsChrimson (n=13) 2. UAS-CsChrimson (n=11)	<0.0001	<0.0001	****
	Number of Peristaltic Backward Waves	Kruskal-Wallis test	1. GH146-GAL4>UAS-CsChrimson (n=12) 2. GH146-GAL4 (n=11) 3. NP225-GAL4>UAS-CsChrimson (n=13) 4. NP225-GAL4 (n=10) 5. NP5288-GAL4>UAS-CsChrimson (n=13) 6. NP5288-GAL4 (n=11) 7. UAS-CsChrimson (n=11)	<0.0001	-	****
	Number of Peristaltic Backward Waves	Dunn's multiple comparisons test	1. GH146-GAL4>UAS-CsChrimson (n=12) 2. GH146-GAL4 (n=11)	<0.0001	<0.0001	***
	Number of Peristaltic Backward Waves	Dunn's multiple comparisons test	1. GH146-GAL4>UAS-CsChrimson (n=12) 2. UAS-CsChrimson (n=11)	<0.0001	<0.0001	****
	Number of Peristaltic Backward Waves	Dunn's multiple comparisons test	1. NP225-GAL4>UAS-CsChrimson (n=13) 2. NP225-GAL4 (n=10)	0.00018	0.00018	***
	Number of Peristaltic Backward Waves	Dunn's multiple comparisons test	1. NP225-GAL4>UAS-CsChrimson (n=13) 2. UAS-CsChrimson (n=11)	<0.0001	<0.0001	****
	Number of Peristaltic Backward Waves	Dunn's multiple comparisons test	1. NP5288-GAL4>UAS-CsChrimson (n=13) 2. NP5288-GAL4 (n=11)	<0.0001	<0.0001	****
	Number of Peristaltic Backward Waves	Dunn's multiple comparisons test	1. NP5288-GAL4>UAS-CsChrimson (n=13) 2. UAS-CsChrimson (n=11)	<0.0001	<0.0001	****

Figure 1D	Mean Translational Velocity	Kruskal-Wallis test	1. GH146-GAL4>UAS-CsChrimson, GH146-QF>QUAS-GAL80 (n=8) 2. GH146-GAL4 (n=11) 3. UAS-CsChrimson (n=11)	<0.0001	-	****
	Mean Translational Velocity	Dunn's multiple comparisons test	1. GH146-GAL4>UAS-CsChrimson, GH146-QF>QUAS-GAL80 (n=8) 2. GH146-GAL4 (n=11)	0.02021	0.02021	*
	Mean Translational Velocity	Dunn's multiple comparisons test	1. GH146-GAL4>UAS-CsChrimson, GH146-QF>QUAS-GAL80 (n=8) 2. UAS-CsChrimson (n=11)	<0.0001	<0.0001	****
	Number of Peristaltic Backward Waves	Kruskal-Wallis test	1. GH146-GAL4>UAS-CsChrimson, GH146-QF>QUAS-GAL80 (n=8) 2. GH146-GAL4 (n=11) 3. UAS-CsChrimson (n=11)	<0.0001	-	****
	Number of Peristaltic Backward Waves	Dunn's multiple comparisons test	1. GH146-GAL4>UAS-CsChrimson, GH146-QF>QUAS-GAL80 (n=8) 2. GH146-GAL4 (n=11)	0.0044	0.0044	**
	Number of Peristaltic Backward Waves	Dunn's multiple comparisons test	1. GH146-GAL4>UAS-CsChrimson, GH146-QF>QUAS-GAL80 (n=8) 2. UAS-CsChrimson (n=11)	<0.0001	<0.0001	****
Figure 1F	Mean Translational Velocity	Mann-Whitney test	1. GH146-GAL4, UAS-hPR:FLP, act5C-FRT-stop-FRT-LexA, LexAop-CsChrimson -RU486 Larva (n=11) 2. GH146-GAL4, UAS-hPR:FLP, act5C-FRT-stop-FRT-LexA, LexAop-CsChrimson +RU486 Larva (n=14)	<0.0001	-	****
	Mean Translational Velocity	Mann-Whitney test	1. GH146-GAL4, UAS-hPR:FLP, act5C-FRT-stop-FRT-LexA, LexAop-CsChrimson -RU486 Adult (n=11) 2. GH146-GAL4, UAS-hPR:FLP, act5C-FRT-stop-FRT-LexA, LexAop-CsChrimson +RU486 Adult (n=14)	<0.0001	-	****
Figure 1G	Mean Translational Velocity	Mann-Whitney test	1. GH146-GAL4>SPARC2-I-CsChrimson, nSyb-PhiC31 No BW Larva (n=7) 2. GH146-GAL4>SPARC2-I-CsChrimson, nSyb-PhiC31 BW Larva (n=13)	<0.0001	-	****
	Mean Translational Velocity	Mann-Whitney test	1. GH146-GAL4>SPARC2-I-CsChrimson, nSyb-PhiC31 No BW Adult (n=7) 2. GH146-GAL4>SPARC2-I-CsChrimson, nSyb-PhiC31 BW Adult (n=13)	0.00018	-	***
Figure 2D	Mean Angular Speed	Mann-Whitney test	1. GH146-GAL4>UAS-CsChrimson, GH146-QF>QUAS-GAL80 Larva (n=8) 2. GH146-GAL4>UAS-CsChrimson, GH146-QF>QUAS-GAL80 Adult (n=18)	<0.0001	-	****

Figure 2E	Absolute Total Angular Change	Mann-Whitney test	1. GH146-GAL4>UAS-CsChrimson, GH146-QF>QUAS-GAL80 Larva (n=8) 2. GH146-GAL4>UAS-CsChrimson, GH146-QF>QUAS-GAL80 Adult (n=18)	<0.0001	-	****
Figure 3A	Mean Translational Velocity	Kruskal-Wallis test	1. R60F09-GAL4>UAS-CsChrimson (n=21) 2. R11E07-GAL4>UAS-CsChrimson (n=11) 3. R11E07-p65.AD&R60F09-GAL4.DBD>UAS-CsChrimson (n=10) 4. GH146-GAL4>UAS-CsChrimson, GH146-QF>QUAS-GAL80 (n=32)	<0.0001	-	****
	Mean Translational Velocity	Dunn's multiple comparisons test	1. GH146-GAL4>UAS-CsChrimson, GH146-QF>QUAS-GAL80 (n=32) 2 R60F09-GAL4>UAS-CsChrimson (n=21)	0.17781	0.17781	n.s.
	Mean Translational Velocity	Dunn's multiple comparisons test	1. GH146-GAL4>UAS-CsChrimson, GH146-QF>QUAS-GAL80 (n=32) 2. R11E07-GAL4>UAS-CsChrimson (n=11)	0.01357	0.02035	*
	Mean Translational Velocity	Dunn's multiple comparisons test	1. GH146-GAL4>UAS-CsChrimson, GH146-QF>QUAS-GAL80 (n=32) 2. R11E07-p65.AD&R60F09-GAL4.DBD>UAS-CsChrimson (n=10)	<0.0001	<0.0001	****
Figure 3D	Mean Translational Velocity	Mann-Whitney test	1. R60F09-GAL4, UAS-hPR:FLP, act5C-FRT-stop-FRT-LexA, LexAop-CsChrimson -RU486 Larva (n=12) 2. R60F09-GAL4, UAS-hPR:FLP, act5C-FRT-stop-FRT-LexA, LexAop-CsChrimson +RU486 Larva (n=11)	<0.0001	-	****
	Mean Translational Velocity	Mann-Whitney test	1. R60F09-GAL4, UAS-hPR:FLP, act5C-FRT-stop-FRT-LexA, LexAop-CsChrimson -RU486 Adult (n=12) 2. R60F09-GAL4, UAS-hPR:FLP, act5C-FRT-stop-FRT-LexA, LexAop-CsChrimson +RU486 Adult (n=11)	<0.0001	-	****
Figure 5L	Cable Length	Kruskal-Wallis test	1. VT020742-p65.AD&R60F09-GAL4.DBD>UAS-CsChrimson (n=10) 2. VT020742-p65.AD&R60F09-GAL4.DBD>UAS-CsChrimson, UAS-EcR$^{DN\text{-}B1\ (W650A)}$ (n=10) 3. VT020742-p65.AD&R60F09-GAL4.DBD>UAS-CsChrimson, UAS-EcR$^{DN\text{-}B1\ (F645A)}$ (n=10) 4. VT020742-p65.AD&R60F09-GAL4.DBD>UAS-CsChrimson, UAS-EcR$^{DN\text{-}A\ (W650A)}$ (n=10) 5. VT020742-p65.AD&R60F09-GAL4.DBD>UAS-CsChrimson, UAS-EcR$^{DN\text{-}A\ (F645A)}$ (n=10)	<0.0001	-	****
	Cable Length	Dunn's multiple comparisons test	1. VT020742-p65.AD&R60F09-GAL4.DBD>UAS-CsChrimson (n=10) 2. VT020742-p65.AD&R60F09-GAL4.DBD>UAS-CsChrimson, UAS-EcR$^{DN\text{-}B1\ (W650A)}$ (n=10)	<0.0001	<0.0001	****
	Cable Length	Dunn's multiple comparisons test	1. VT020742-p65.AD&R60F09-GAL4.DBD>UAS-CsChrimson (n=10) 2. VT020742-p65.AD&R60F09-GAL4.DBD>UAS-CsChrimson, UAS-EcR$^{DN\text{-}B1\ (F645A)}$ (n=10)	0.00576	0.00768	**

	Cable Length	Dunn's multiple comparisons test	1. VT020742-p65.AD&R60F09-GAL4.DBD>UAS-CsChrimson (n=10) 2. VT020742-p65.AD&R60F09-GAL4.DBD>UAS-CsChrimson, UAS-EcR$^{DN\text{-}A\ (W650A)}$ (n=10)	<0.0001	<0.0001	****
	Cable Length	Dunn's multiple comparisons test	1. VT020742-p65.AD&R60F09-GAL4.DBD>UAS-CsChrimson (n=10) 2. VT020742-p65.AD&R60F09-GAL4.DBD>UAS-CsChrimson, UAS-EcR$^{DN\text{-}A\ (F645A)}$ (n=10)	0.025	0.025	*
Figure 5M	Number of branch points	Kruskal-Wallis test	1. VT020742-p65.AD&R60F09-GAL4.DBD>UAS-CsChrimson (n=10) 2. VT020742-p65.AD&R60F09-GAL4.DBD>UAS-CsChrimson, UAS-EcR$^{DN\text{-}B1\ (W650A)}$ (n=10) 3. VT020742-p65.AD&R60F09-GAL4.DBD>UAS-CsChrimson, UAS-EcR$^{DN\text{-}B1\ (F645A)}$ (n=10) 4. VT020742-p65.AD&R60F09-GAL4.DBD>UAS-CsChrimson, UAS-EcR$^{DN\text{-}A\ (W650A)}$ (n=10) 5. VT020742-p65.AD&R60F09-GAL4.DBD>UAS-CsChrimson, UAS-EcR$^{DN\text{-}A\ (F645A)}$ (n=10)	<0.0001	-	****
	Number of branch points	Dunn's multiple comparisons test	1. VT020742-p65.AD&R60F09-GAL4.DBD>UAS-CsChrimson (n=10) 2. VT020742-p65.AD&R60F09-GAL4.DBD>UAS-CsChrimson, UAS-EcR$^{DN\text{-}B1\ (W650A)}$ (n=10)	<0.0001	<0.0001	****
	Number of branch points	Dunn's multiple comparisons test	1. VT020742-p65.AD&R60F09-GAL4.DBD>UAS-CsChrimson (n=10) 2. VT020742-p65.AD&R60F09-GAL4.DBD>UAS-CsChrimson, UAS-EcR$^{DN\text{-}B1\ (F645A)}$ (n=10)	0.01321	0.01321	*
	Number of branch points	Dunn's multiple comparisons test	1. VT020742-p65.AD&R60F09-GAL4.DBD>UAS-CsChrimson (n=10) 2. VT020742-p65.AD&R60F09-GAL4.DBD>UAS-CsChrimson, UAS-EcR$^{DN\text{-}A\ (W650A)}$ (n=10)	<0.0001	<0.0001	****
	Number of branch points	Dunn's multiple comparisons test	1. VT020742-p65.AD&R60F09-GAL4.DBD>UAS-CsChrimson (n=10) 2. VT020742-p65.AD&R60F09-GAL4.DBD>UAS-CsChrimson, UAS-EcR$^{DN\text{-}A\ (F645A)}$ (n=10)	0.00314	0.00418	**
Figure 5N	Convex Hull Size	Kruskal-Wallis test	1. VT020742-p65.AD&R60F09-GAL4.DBD>UAS-CsChrimson (n=10) 2. VT020742-p65.AD&R60F09-GAL4.DBD>UAS-CsChrimson, UAS-EcR$^{DN\text{-}B1\ (W650A)}$ (n=10) 3. VT020742-p65.AD&R60F09-GAL4.DBD>UAS-CsChrimson, UAS-EcR$^{DN\text{-}B1\ (F645A)}$ (n=10) 4. VT020742-p65.AD&R60F09-GAL4.DBD>UAS-CsChrimson, UAS-EcR$^{DN\text{-}A\ (W650A)}$ (n=10) 5. VT020742-p65.AD&R60F09-GAL4.DBD>UAS-CsChrimson, UAS-EcR$^{DN\text{-}A\ (F645A)}$ (n=10)	<0.0001	-	****
	Convex Hull Size	Dunn's multiple comparisons test	1. VT020742-p65.AD&R60F09-GAL4.DBD>UAS-CsChrimson (n=10) 2. VT020742-p65.AD&R60F09-GAL4.DBD>UAS-CsChrimson, UAS-EcR$^{DN\text{-}B1\ (W650A)}$ (n=10)	<0.0001	<0.0001	****
	Convex Hull Size	Dunn's multiple comparisons test	1. VT020742-p65.AD&R60F09-GAL4.DBD>UAS-CsChrimson (n=10) 2. VT020742-p65.AD&R60F09-GAL4.DBD>UAS-CsChrimson, UAS-EcR$^{DN\text{-}B1\ (F645A)}$ (n=10)	<0.0001	<0.0001	****

	Convex Hull Size	Dunn's multiple comparisons test	1. VT020742-p65.AD&R60F09-GAL4.DBD>UAS-CsChrimson (n=10) 2. VT020742-p65.AD&R60F09-GAL4.DBD>UAS-CsChrimson, UAS-EcR$^{DN\text{-}A\ (W650A)}$ (n=10)	0.00114	0.00152	**
	Convex Hull Size	Dunn's multiple comparisons test	1. VT020742-p65.AD&R60F09-GAL4.DBD>UAS-CsChrimson (n=10) 2. VT020742-p65.AD&R60F09-GAL4.DBD>UAS-CsChrimson, UAS-EcR$^{DN\text{-}A\ (F645A)}$ (n=10)	0.0066	0.0066	**
Figure 5O	Mean Translational Velocity	Kruskal-Wallis test	1. VT020742-p65.AD&R60F09-GAL4.DBD>UAS-CsChrimson (II) (n=25) 1. VT020742-p65.AD&R60F09-GAL4.DBD>UAS-CsChrimson (III) (n=33) 2. VT020742-p65.AD&R60F09-GAL4.DBD>UAS-CsChrimson, UAS-EcR$^{DN\text{-}B1\ (W650A)}$ (n=34) 3. VT020742-p65.AD&R60F09-GAL4.DBD>UAS-CsChrimson, UAS-EcR$^{DN\text{-}B1\ (F645A)}$ (n=33) 4. VT020742-p65.AD&R60F09-GAL4.DBD>UAS-CsChrimson, UAS-EcR$^{DN\text{-}A\ (W650A)}$ (n=31) 5. VT020742-p65.AD&R60F09-GAL4.DBD>UAS-CsChrimson, UAS-EcR$^{DN\text{-}A\ (F645A)}$ (n=29)	<0.0001	-	****
	Mean Translational Velocity	Dunn's multiple comparisons test	1. VT020742-p65.AD&R60F09-GAL4.DBD>UAS-CsChrimson (II) (n=25) 2. VT020742-p65.AD&R60F09-GAL4.DBD>UAS-CsChrimson, UAS-EcR$^{DN\text{-}B1\ (W650A)}$ (n=34)	<0.0001	<0.0001	****
	Mean Translational Velocity	Dunn's multiple comparisons test	1. VT020742-p65.AD&R60F09-GAL4.DBD>UAS-CsChrimson (III) (n=33) 2. VT020742-p65.AD&R60F09-GAL4.DBD>UAS-CsChrimson, UAS-EcR$^{DN\text{-}B1\ (F645A)}$ (n=33)	<0.0001	<0.0001	****
	Mean Translational Velocity	Dunn's multiple comparisons test	1. VT020742-p65.AD&R60F09-GAL4.DBD>UAS-CsChrimson (III) (n=33) 2. VT020742-p65.AD&R60F09-GAL4.DBD>UAS-CsChrimson, UAS-EcR$^{DN\text{-}A\ (W650A)}$ (n=31)	<0.0001	<0.0001	****
	Mean Translational Velocity	Dunn's multiple comparisons test	1. VT020742-p65.AD&R60F09-GAL4.DBD>UAS-CsChrimson (III) (n=33) 2. VT020742-p65.AD&R60F09-GAL4.DBD>UAS-CsChrimson, UAS-EcR$^{DN\text{-}A\ (F645A)}$ (n=29)	0.0005	0.0005	***
	Standardized z-score of Mean Translational Velocity	D'Agostino&Pearson normality test	VT020742-p65.AD&R60F09-GAL4.DBD>UAS-CsChrimson - Larva (n=16)	0.54991	-	n.s.
		D'Agostino&Pearson normality test	VT020742-p65.AD&R60F09-GAL4.DBD>UAS-CsChrimson - Adult (n=16)	0.82596	-	n.s.
		D'Agostino&Pearson normality test	VT020742-p65.AD&R60F09-GAL4.DBD>UAS-CsChrimson, UAS-EcR$^{DN\text{-}B1\ (W650A)}$ - Larva (n=16)	0.8071	-	n.s.
		D'Agostino&Pearson normality test	VT020742-p65.AD&R60F09-GAL4.DBD>UAS-CsChrimson, UAS-EcR$^{DN\text{-}B1\ (W650A)}$ - Adult (n=16)	0.26021	-	n.s.

Figure 5P	Standardized z-score of Mean Translational Velocity	Repeated measures two-way ANOVA	Main effect: Developmental stage (larva, n=32; adult, n=32)	>0.99999	>0.99999	n.s.
			Main effect: Genotype (VT020742-p65.AD&R60F09-GAL4.DBD>UAS-CsChrimson, n=32; VT020742-p65.AD&R60F09-GAL4.DBD>UAS-CsChrimson, UAS-EcR$^{DN\text{-}B1\ (W650A)}$, n=32)	0.00265	0.00398	**
			Interaction effect: Developmental stage (larva, n=32; adult, n=32) X Genotype (VT020742-p65.AD&R60F09-GAL4.DBD>UAS-CsChrimson, n=32; VT020742-p65.AD&R60F09-GAL4.DBD>UAS-CsChrimson, UAS-EcR$^{DN\text{-}B1\ (W650A)}$, n=32)	<0.0001	<0.0001	****
Figure S1B	Standardized z-score of Mean Translational Velocity	D'Agostino&Pearson normality test	GH146-GAL4, UAS-hPR:FLP, act5C-FRT-stop-FRT-LexA, LexAop-CsChrimson -RU486 - Larva (n=11)	0.15235	-	n.s.
		D'Agostino&Pearson normality test	GH146-GAL4, UAS-hPR:FLP, act5C-FRT-stop-FRT-LexA, LexAop-CsChrimson +RU486 - Larva (n=14)	0.86634	-	n.s.
		D'Agostino&Pearson normality test	GH146-GAL4, UAS-hPR:FLP, act5C-FRT-stop-FRT-LexA, LexAop-CsChrimson -RU486 - Adult (n=11)	0.1516	-	n.s.
		D'Agostino&Pearson normality test	GH146-GAL4, UAS-hPR:FLP, act5C-FRT-stop-FRT-LexA, LexAop-CsChrimson +RU486 - Adult (n=14)	0.05654	-	n.s.
	Standardized z-score of Mean Translational Velocity	Repeated measures two-way ANOVA	Main effect: Developmental stage (larva, n=25; adult, n=25)	0.97342	0.97342	n.s.
			Main effect: RU486 treatment (+RU486, n=28; -RU486, n=22)	<0.0001	<0.0001	****
			Interaction effect: Developmental stage (larva, n=25; adult, n=25) X RU486 treatment (+RU486, n=28; -RU486, n=22)	0.78149	0.97342	n.s.
Figure S2D	Mean Translational Velocity	Mann-Whitney test	1. R60F09-LexA>LexAop-CsChrimson, GH146-GAL4>UAS-GtACR2 No background blue light (n=16) 2. R60F09-LexA>LexAop-CsChrimson, GH146-GAL4>UAS-GtACR2 Background blue light (n=20)	<0.0001	-	****
Figure S2E	Mean Translational Velocity	Mann-Whitney test	1. GH146-GAL4>UAS-CsChrimson, R60F09-LexA (n=20) 2. GH146-GAL4>UAS-CsChrimson, R60F09-LexA>LexAop-TNT (n=59)	<0.0001	-	****
Figure S2G	Mean Translational Velocity	Kruskal-Wallis test	1. R60F09-GAL4>UAS-CsChrimson (n=21) 2. Otd-FLP, tub-FRT-STOP-FRT-GAL80 (n=22) 3. R60F09-GAL4>UAS-CsChrimson, Otd-FLP, tub-FRT-STOP-FRT-GAL80 (n=25)	<0.0001	-	****
	Mean Translational Velocity	Dunn's multiple comparisons test	1. R60F09-GAL4>UAS-CsChrimson (n=21) 2. Otd-FLP, tub-FRT-STOP-FRT-GAL80 (n=22)	<0.0001	<0.0001	****
	Mean Translational Velocity	Dunn's multiple comparisons test	1. R60F09-GAL4>UAS-CsChrimson (n=21) 2. R60F09-GAL4>UAS-CsChrimson, Otd-FLP, tub-FRT-STOP-FRT-GAL80 (n=25)	0.07809	0.07809	n.s.
	Mean Translational Velocity	Dunn's multiple comparisons test	1. Otd-FLP, tub-FRT-STOP-FRT-GAL80 (n=22) 2. R60F09-GAL4>UAS-CsChrimson, Otd-FLP, tub-FRT-STOP-FRT-GAL80 (n=25)	<0.0001	<0.0001	****

Figure S3A	Standardized z-score of Mean Translational Velocity	D'Agostino&Pearson normality test	R60F09-GAL4, UAS-hPR:FLP, act5C-FRT-stop-FRT-LexA, LexAop-CsChrimson -RU486 - Larva (n=12)	0.9558	-	n.s.
		D'Agostino&Pearson normality test	R60F09-GAL4, UAS-hPR:FLP, act5C-FRT-stop-FRT-LexA, LexAop-CsChrimson +RU486 - Larva (n=11)	0.35988	-	n.s.
		D'Agostino&Pearson normality test	R60F09-GAL4, UAS-hPR:FLP, act5C-FRT-stop-FRT-LexA, LexAop-CsChrimson -RU486 - Adult (n=12)	0.73671	-	n.s.
		D'Agostino&Pearson normality test	R60F09-GAL4, UAS-hPR:FLP, act5C-FRT-stop-FRT-LexA, LexAop-CsChrimson +RU486 - Adult (n=11)	0.01331	-	*
	Standardized z-score of Mean Translational Velocity	Repeated measures two-way ANOVA	Main effect: Developmental stage (larva, n=25; adult, n=25)	0.98443	0.98443	n.s.
			Main effect: RU486 treatment (+RU486, n=28; -RU486, n=22)	<0.0001	<0.0001	****
			Interaction effect: Developmental stage (larva, n=25; adult, n=25) X RU486 treatment (+RU486, n=28; -RU486, n=22)	0.65451	0.98176	n.s.
Figure S3D	Mean Translational Velocity	Kruskal-Wallis test	1. VT020742-p65.AD&R60F09-GAL4.DBD>UAS-CsChrimson (n=8) 2. VT032768-p65.AD&R60F09-GAL4.DBD>UAS-CsChrimson (n=11) 3. VT020742-p65.AD&R60F09-GAL4.DBD (n=13) 4. VT032768-p65.AD&R60F09-GAL4.DBD (n=12) 5. UAS-CsChrimson (n=11)	<0.0001	-	****
	Mean Translational Velocity	Dunn's multiple comparisons test	1. VT020742-p65.AD&R60F09-GAL4.DBD>UAS-CsChrimson (n=8) 2. VT020742-p65.AD&R60F09-GAL4.DBD (n=13)	0.00019	0.00039	***
	Mean Translational Velocity	Dunn's multiple comparisons test	1. VT020742-p65.AD&R60F09-GAL4.DBD>UAS-CsChrimson (n=8) 2. UAS-CsChrimson (n=11)	0.00354	0.00354	**
	Mean Translational Velocity	Dunn's multiple comparisons test	1. VT032768-p65.AD&R60F09-GAL4.DBD>UAS-CsChrimson (n=11) 2. VT032768-p65.AD&R60F09-GAL4.DBD (n=12)	<0.0001	<0.0001	****
	Mean Translational Velocity	Dunn's multiple comparisons test	1. VT032768-p65.AD&R60F09-GAL4.DBD>UAS-CsChrimson (n=11) 2. UAS-CsChrimson (n=11)	0.00029	0.00039	***
	Number of Peristaltic Backward Waves	Kruskal-Wallis test	1. VT020742-p65.AD&R60F09-GAL4.DBD>UAS-CsChrimson (n=8) 2. VT032768-p65.AD&R60F09-GAL4.DBD>UAS-CsChrimson (n=11) 3. VT020742-p65.AD&R60F09-GAL4.DBD (n=13) 4. VT032768-p65.AD&R60F09-GAL4.DBD (n=12) 5. UAS-CsChrimson (n=11)	<0.0001	-	****

	Number of Peristaltic Backward Waves	Dunn's multiple comparisons test	1. VT020742-p65.AD&R60F09-GAL4.DBD>UAS-CsChrimson (n=8) 2. VT020742-p65.AD&R60F09-GAL4.DBD (n=13)	<0.0001	<0.0001	****
	Number of Peristaltic Backward Waves	Dunn's multiple comparisons test	1. VT020742-p65.AD&R60F09-GAL4.DBD>UAS-CsChrimson (n=8) 2. UAS-CsChrimson (n=11)	<0.0001	<0.0001	****
	Number of Peristaltic Backward Waves	Dunn's multiple comparisons test	1. VT032768-p65.AD&R60F09-GAL4.DBD>UAS-CsChrimson (n=11) 2. VT032768-p65.AD&R60F09-GAL4.DBD (n=12)	<0.0001	<0.0001	****
	Number of Peristaltic Backward Waves	Dunn's multiple comparisons test	1. VT032768-p65.AD&R60F09-GAL4.DBD>UAS-CsChrimson (n=11) 2. UAS-CsChrimson (n=11)	<0.0001	<0.0001	****
Figure S3E	Mean Translational Velocity	Kruskal-Wallis test	1. VT020742-p65.AD&R60F09-GAL4.DBD>UAS-CsChrimson (n=38) 2. VT032768-p65.AD&R60F09-GAL4.DBD>UAS-CsChrimson (n=31) 3. VT020742-p65.AD&R60F09-GAL4.DBD (n=32) 4. VT032768-p65.AD&R60F09-GAL4.DBD (n=15) 5. UAS-CsChrimson (n=32)	<0.0001	-	****
	Mean Translational Velocity	Dunn's multiple comparisons test	1. VT020742-p65.AD&R60F09-GAL4.DBD>UAS-CsChrimson (n=38) 2. VT020742-p65.AD&R60F09-GAL4.DBD (n=32)	<0.0001	<0.0001	****
	Mean Translational Velocity	Dunn's multiple comparisons test	1. VT020742-p65.AD&R60F09-GAL4.DBD>UAS-CsChrimson (n=38) 2. UAS-CsChrimson (n=32)	<0.0001	<0.0001	****
	Mean Translational Velocity	Dunn's multiple comparisons test	1. VT032768-p65.AD&R60F09-GAL4.DBD>UAS-CsChrimson (n=31) 2. VT032768-p65.AD&R60F09-GAL4.DBD (n=15)	<0.0001	<0.0001	****
	Mean Translational Velocity	Dunn's multiple comparisons test	1. VT032768-p65.AD&R60F09-GAL4.DBD>UAS-CsChrimson (n=31) 2. UAS-CsChrimson (n=32)	<0.0001	<0.0001	****
Figure S3F	Mean Translational Velocity	Mann-Whitney test	1. VT020742-p65.AD&R60F09-GAL4.DBD>UAS-CsChrimson, MDN-LexA (n=16) 2. VT020742-p65.AD&R60F09-GAL4.DBD>UAS-CsChrimson, MDN-LexA>LexAop-TNT(n=19)	0.01108	-	*
Figure S3G	Mean Angular Speed	Mann-Whitney test	1. VT020742-p65.AD&R60F09-GAL4.DBD>UAS-CsChrimson, MDN-LexA (n=9) 2. VT020742-p65.AD&R60F09-GAL4.DBD>UAS-CsChrimson, MDN-LexA>LexAop-TNT(n=15)	0.63989	-	n.s.
Figure S3H	Absolute Total Angular Change	Mann-Whitney test	1. VT020742-p65.AD&R60F09-GAL4.DBD>UAS-CsChrimson, MDN-LexA (n=9) 2. VT020742-p65.AD&R60F09-GAL4.DBD>UAS-CsChrimson, MDN-LexA>LexAop-TNT(n=15)	0.68238	-	n.s.